

Article

Divergent Structure-Activity Relationships of Structurally Similar Acetylcholinesterase Inhibitors

C. David Andersson, Nina Forsgren, Christine Akfur, Anders Allgardsson, Lotta Berg, Cecilia Engdahl, Weixing Qian, Fredrik Johan Ekström, and Anna Linusson

J. Med. Chem., **Just Accepted Manuscript** • DOI: 10.1021/jm400990p • Publication Date (Web): 28 Aug 2013

Downloaded from <http://pubs.acs.org> on August 31, 2013

Just Accepted

"Just Accepted" manuscripts have been peer-reviewed and accepted for publication. They are posted online prior to technical editing, formatting for publication and author proofing. The American Chemical Society provides "Just Accepted" as a free service to the research community to expedite the dissemination of scientific material as soon as possible after acceptance. "Just Accepted" manuscripts appear in full in PDF format accompanied by an HTML abstract. "Just Accepted" manuscripts have been fully peer reviewed, but should not be considered the official version of record. They are accessible to all readers and citable by the Digital Object Identifier (DOI®). "Just Accepted" is an optional service offered to authors. Therefore, the "Just Accepted" Web site may not include all articles that will be published in the journal. After a manuscript is technically edited and formatted, it will be removed from the "Just Accepted" Web site and published as an ASAP article. Note that technical editing may introduce minor changes to the manuscript text and/or graphics which could affect content, and all legal disclaimers and ethical guidelines that apply to the journal pertain. ACS cannot be held responsible for errors or consequences arising from the use of information contained in these "Just Accepted" manuscripts.



ACS Publications
High quality. High impact.

Journal of Medicinal Chemistry is published by the American Chemical Society, 1155 Sixteenth Street N.W., Washington, DC 20036
Published by American Chemical Society. Copyright © American Chemical Society. However, no copyright claim is made to original U.S. Government works, or works produced by employees of any Commonwealth realm Crown government in the course of their duties.

Divergent Structure-Activity Relationships of Structurally Similar Acetylcholinesterase Inhibitors

C. David Andersson,[#] Nina Forsgren,[□] Christine Akfur,[□] Anders Allgardsson,[□] Lotta Berg,[#] Cecilia Engdahl,^{#,□} Weixing Qian,[#] Fredrik Ekström,^{□,} and Anna Linusson.^{#,*}*

[#] Department of Chemistry, Umeå University, SE-901 87 Umeå, Sweden. [□] Swedish Defense Research Agency, CBRN Defense and Security, SE-906 21 Umeå, Sweden.

KEYWORDS: Acetylcholinesterase, molecular recognition, structure-activity relationship, peripheral anionic site, aromatic interactions, face-to-face, edge-to-face, isothermal titration calorimetry.

ABSTRACT

The molecular interactions between the enzyme acetylcholinesterase (AChE) and two compound classes consisting of *N*-[2-(diethylamino)-ethyl]-benzenesulfonamides and *N*-[2-(diethylamino)-ethyl]-benzenemethanesulfonamides have been investigated using organic synthesis, enzymatic assays, X-ray crystallography, and thermodynamic profiling. The inhibitors' aromatic properties were varied to establish structure-activity relationships (SAR) between the inhibitors and the peripheral anionic site (PAS) of AChE. The two structurally similar compound classes proved to have distinctly divergent SARs in terms of their inhibition capacity of AChE. Eight X-ray structures revealed that the two sets have different conformations in PAS. Furthermore, thermodynamic profiles of the binding between compounds and AChE revealed class-dependent differences of the entropy/enthalpy contributions to the free energy of binding. Further development of the entropy-favored compound class resulted in the synthesis of the most potent inhibitor, and an extension beyond the established SARs. The divergent SARs will be utilized to develop reversible inhibitors of AChE into reactivators of nerve agent inhibited AChE.

INTRODUCTION

The interaction between small organic molecules and proteins plays a key role in most biological processes. To obtain a better understanding of this event, the fundamental mechanisms governing molecular recognition need to be further clarified and generalized. In this medicinal chemistry program we investigated the binding between the enzyme acetylcholinesterase (AChE) and a set of small organic molecules by using a combination of organic synthesis, enzymatic assays, X-ray crystallography, and thermodynamic profiling. The compounds were specifically designed to probe the non-covalent interactions present between the inhibitors and the protein, while aiming to discover and develop compounds for AChE inhibition as well as compounds acting as reactivators of nerve agent inhibited AChE.

AChE is an essential enzyme that terminates cholinergic transmission by the hydrolysis of the neurotransmitter acetylcholine (ACh).¹ Reversible AChE inhibitors are in use for symptomatic treatment of *e.g.*, Huntington's disease,² and Alzheimer's disease (AD),³⁻⁴ where increased ACh levels results in reduced disease symptoms. AChE inhibitors may also act as toxins, *e.g.*, organophosphorus-based nerve agents, which block the enzymatic activity by covalently binding to the catalytic serine residue. The lethal condition caused by these agents may be reversed by treatment with reactivators (antidotes) that are capable of binding in the active site gorge and cleave the bond between the enzyme and the nerve agent, thereby restoring the enzymatic activity. Both AChE inhibitors currently used in disease treatment and reactivators used to treat nerve agent intoxication suffer from limited efficacy due to *e.g.*, limited blood-brain barrier penetration capability,⁵ and they are commonly associated with adverse effects⁶ making the search for new AChE inhibitors warranted. The discovery of compounds binding to AChE may result in new therapeutics but can also be utilized in the development of new reactivators that can be synthesized from reversible inhibitors by the introduction of a nucleophilic chemical group.⁷ Additionally, a more thorough understanding of the mechanisms governing the molecular recognition in AChE may assist in avoiding off-target effects of drugs aimed at other targets in the body.

The active site of AChE forms a deep and sterically confined gorge that serves as the binding site for both natural and synthetic ligands. The gorge structure is conserved among the extensively studied *Mus musculus* AChE (*mAChE*),⁸ *Torpedo californica* AChE,⁹ and the recently solved structure for *human* AChE (*hAChE*).¹⁰ The binding site is composed of two sub-sites; the peripheral anionic site (PAS) corresponds to the entrance of the active site gorge, and the catalytic site (CAS) is situated close to the base of the active site gorge. Common features of compounds binding to AChE are basic- or permanently charged nitrogens and aromatic systems that can form interactions to one, or both, of the subsites. Galanthamine¹¹ (half-maximal inhibitory concentration (IC_{50}) in *hAChE* of 2.01 μM)¹² and huperzine¹³ (IC_{50} of 0.082 μM in *mAChE*)¹⁴ are both examples of AD drugs that bind to the CAS, while propidium iodide (IC_{50} in *mAChE* of 1.1 μM)¹⁵ binds in the PAS region.⁸ Examples of inhibitors that bind to PAS and CAS simultaneously are some tetracycline-based compounds displaying an IC_{50} in the nano-molar region (*hAChE*), tacrin analogues¹⁶⁻¹⁹ including the structurally symmetrical inhibitor bis-tacrine^{16, 20} and the non-symmetrical tacrine-containing TZ2PA6 (K_d in *mAChE* of 0.41 nM).²¹⁻²² The well-studied class of benzylamines *e.g.*, donepezil, which is a low nano-molar binder for AChE also used in symptomatic treatment of AD (Figure 1), binds with a basic nitrogen in the CAS and an aromatic system in the PAS.²³⁻²⁷ HI-6 (Figure 1) is an example of a reactivator that binds to both the CAS and the PAS with its two positively charged aromatic rings that has an IC_{50} for *hAChE* of 66 μM .^{28,29} This list of examples is by no means comprehensive and we also refer to reviews on AChE inhibitors.³⁰⁻³²

Crystal structures of AChE•inhibitor complexes have shown that AChE inhibitors commonly interact with the gorge residues *via* arene–arene interactions. Aromatic ring-stacking “face-to-face” interactions are present in complexes with most tacrine analogues that bind to AChE, as well as in the complexes with donepezil^{25, 33} and HI-6.²⁹ “Edge-to-face” interactions are less common but have been observed in, for example, the PAS region of the complex with the non-symmetrical compound TZ2PA6.²² Alterations in the aromatic systems of ligands may lead to significant changes in affinity and binding mode in general,³⁴ and have been shown for compounds binding to AChE.^{23-24, 26-27, 35-38} Changes can be

introduced by varying arene-substituents resulting in a different overall electrostatic nature of the aromatic ring by introducing dipole-moments as well as by altering the van der Waals surfaces.³⁹⁻⁴¹

In this study, we have designed a set of compounds aimed at exploring the effects of modifying the PAS-binding moiety of an inhibitor of AChE previously identified by us in a high-throughput screening (HTS) campaign (compound **1**, Figure 1).⁴² The objective of the study was to investigate the structure-activity relationships (SAR) and the potential to optimize the PAS-binding moiety for increased binding affinity using extensive biochemical and structural characterizations; with the aim to use the results in future research for new reactivators of nerve agent inhibited AChE.

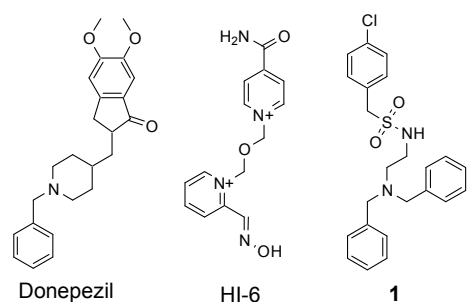


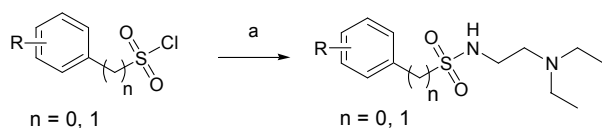
Figure 1. The chemical structures of donepezil, HI-6, and the hit identified in the HTS campaign targeting *h*AChE (**1**).

RESULTS AND DISCUSSION

Design of AChE Inhibitors with a focus on PAS binding. Starting from compound **1** (Figure 1), structurally simplified first-generation analogues were designed for evaluation in *m*AChE using well established experimental protocols for both kinetics and crystallography. Based on the hypothesis that the *para*-chloro benzyl and the tertiary amine of **1** would bind in PAS and CAS, respectively, we simplified the *N,N*-dibenzylamine of **1** to a *N,N*-diethylamine and the substitution pattern on the phenylmethanesulfonamide were varied resulting in different overall aromatic ring electrostatic potential (*e.g.*, electron donating and withdrawing substituents) and van der Waals volume (Table 1).

Seven “benzylic” *N*-[2-(diethylamino)-ethyl]-benzenesulfonamides and twelve “non-benzylic” *N*-[2-(diethylamino)-ethyl]-benzenesulfonamides were synthesized in a one-step reaction forming the sulfonamide from the corresponding sulfonyl chloride and *N,N*-diethylethylene-diamine (Scheme 1).

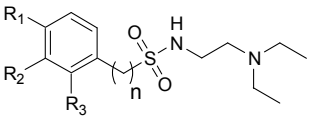
Scheme 1. General synthesis of the AChE inhibitors included in the study^a



^aReagents and conditions: (a) CH₂Cl₂, *N,N*-diethylethylene-diamine, 0 °C → rt, 4 h.

The inhibitory effect of the benzene- and benzenemethane sulfonamides on AChE. The inhibitory effect of the compounds were evaluated on two occasions (two bioreplicates) on independently expressed and purified *m*AChE using the Ellman assay,⁴³ and the results are presented in Table 1 (details are given in the Supporting Information). The bioreplicates gave statistically coherent results, and only the results from bioreplicate B will therefore be discussed henceforth. The inhibitors displayed a range in potency between an *IC*₅₀ of 7 μM and 139 μM. This is comparable to the potency of many currently used reactivators, *e.g.*, HI-6.²⁸ Notably, representatives of both benzylic- and non-benzylic compounds were among the most potent inhibitors (*cf.* **8** and **11**). The SAR conclusions, however, are different for the two compound classes.

Table 1. Inhibition of the enzymatic activity of *m*AChE for compounds in set 1.

						
Bioreplicate B						
ID	<i>n</i>	R1	R2	R3	<i>IC</i> ₅₀ (μM)	95% CI (μM) ^a
2	1	H	H	H	139	122 - 158
3	1	CH ₃	H	H	49	41 - 58

1	4	1	F	H	H	40	34 - 46
2	5	1	Cl	H	H	12	11 - 13
3							
4	6	1	CF ₃	H	H	12	10-14
5							
6	7	1	Br	H	H	10	9-11
7							
8	8	1	Cl	Cl	H	7	6 - 8
9							
10	9	0	H	H	H	31	27 - 36
11							
12	10	0	H	H	F	41	36 - 46
13							
14	11	0	H	OCH ₃	H	7	6 - 8
15							
16	12	0	H	CF ₃	H	22	19 - 24
17							
18	13	0	H	Cl	H	18	15-20
19							
20	14	0	OCH ₃	H	H	119	97 - 145
21							
22	15	0	CH ₃	H	H	135	117 - 156
23							
24	16	0	F	H	H	62	54 - 70
25							
26	17	0	Cl	H	H	88	74 - 106
27							
28	18	0	NO ₂	H	H	95	81 - 111
29							
30	19	0	Cl	H	F	91	80 - 103
31							
32	20	0	F	F	H	50	40 - 63
33							
34							

^a 95% confidence interval calculated from at least 4 replicates.

SAR analysis of benzylic and non-benzylic inhibitors. The SAR of the benzylic inhibitors (Table 1) gave a clear indication that a substituent in the *para*-position was beneficial for the potency while the unsubstituted compound **2** was the least potent. Regarding the electronic properties of the substituents on the aromatic ring, the electron-withdrawing *para*-chloro or *para*- and *meta*-chloro (**5** and **8**, respectively) proved to be more beneficial than the weakly electron-donating methyl-group (**3**). *Para*-trifluoromethyl substituted inhibitor **6** displayed the same potency as the *para*-chloro compound **5**, indicating that increasing the electron-withdrawing capacity of the substituent might not be more beneficial for potency. A trend in the *para*-halogenated inhibitors could be seen, where bromine (**7**)

gave the most potent compound followed by chlorine (**5**) and fluorine (**4**) in decreasing potency order, which may be an effect of decreasing the van der Waals volume of the substituent.

Different SAR conclusions were drawn from the analysis of the non-benzylic inhibitors (Table 1) compared to the benzylic compounds. In contrast to the benzylic compounds, the electron donating or withdrawing capabilities had little influence, although the position of the substituent on the aromatic ring proved critical for the potency of the compounds. The presence of a *meta*-substituent was favorable and the most potent inhibitor was *meta*-methoxy substituted compound **11**, while a *para*-substituent proved unfavorable (*cf.* *para*-methoxy in **14** and *para*-nitro in **18**). There was an indication that a smaller substituent, such as fluorine, was less disadvantageous since inhibitors with this substituent (**16** and **20**) had slightly lower IC_{50} than the other *para*-substituted inhibitors. *Ortho*-fluoro substituted and unsubstituted compounds were equipotent inhibitors (**10** and **9**, respectively), and were slightly more potent than the most potent *para*-substituted inhibitor (**20**).

Previously, the potency of donepezil²⁶ and donepezil-like compounds in AChE inhibition have been examined *via* substituent replacements on the indanone³⁵ or the corresponding PAS-binding moieties in similar molecules.^{23-24, 27, 35-38} These studies showed, in agreement with ours, that altering the presumed PAS-binding moiety has a great effect on the potency, and that electrostatics and van der Waals surfaces, *i.e.*, the lowest unoccupied molecular orbital energy,³⁸ and Lennard-Jones potentials⁴⁴ may be used to explain some of these effects. These conclusions were, however, not supported by X-ray crystallography data.

The thermodynamic binding-profile of the inhibitors. The thermodynamic profiles of the binding between *m*AChE and two benzylic (**5**; *para*-chloro and **6**; *para*-trifluoromethyl) and two non-benzylic (**12**; *meta*-trifluoromethyl, and **13**; *meta*-chloro) inhibitors were determined using ITC (Figure 2). These compounds were selected for further characterization since they have similar substitution patterns (and thus presumably similar solvation properties) and a comparable inhibition potency for *m*AChE. ITC heat-diagrams and titration curve-fitting are presented in the Supporting Information.

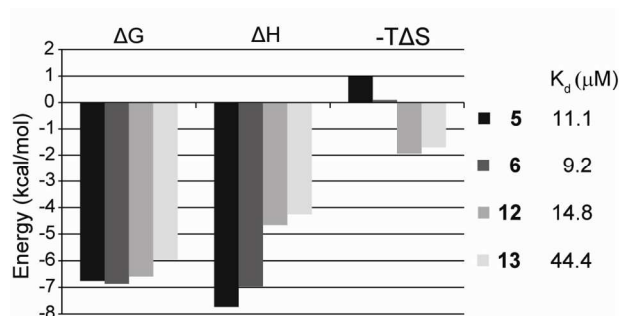


Figure 2. Thermodynamic parameters and dissociation constants measured with ITC for two benzylic (**5**; *para*-chloro and **6**; *para*-trifluoromethyl) and two non-benzylic (**12**; *meta*-trifluoromethyl and **13**; *meta*-chloro) inhibitors of *m*AChE.

Inhibitors **5**, **6** and **12** bound equally strong to *m*AChE, both in terms of the change in Gibbs free energy (ΔG) and dissociation constant (K_d), while **13** bound somewhat weaker (Figure 2). Benzylic inhibitors **5** and **6** had a ΔG of -6.8 and -6.9 kcal/mol, respectively, while non-benzylic **12** and **13** had a ΔG of -6.6 and -6.0 kcal/mol, respectively. Clear differences between the two inhibitor groups emerged when the ΔG was decomposed into enthalpy (ΔH) and entropy (ΔS) components. The benzylic compounds displayed a more favorable enthalpic component while the entropy component was unfavorable. The non-benzylic compounds clearly had beneficial entropy components, where a large proportion of the binding energy came from an entropy gain upon binding. This indicates that the benzylic compounds have more direct and specific enthalpy-driven interactions with *m*AChE and may be less flexible upon binding, while the non-benzylic inhibitors causes a gain in entropy through increased flexibility and/or affecting water molecules *via* the hydrophobic effect.⁴⁵ The fact that the four compounds have different entropy/enthalpy contributions but roughly the same ΔG can be explained by the entropy-enthalpy compensation phenomenon,⁴⁶ which we have reported before for a pair of enantiomeric inhibitors of AChE.⁴⁷

X-ray crystallography of AChE inhibitors. The bioactive conformations of seven of the inhibitors (**3**, **4**, **5**, **10**, **11**, **12**, and **17**) were determined by X-ray crystallography at resolutions ranging from 2.1 to 2.8 Å. The crystal structures showed that the inhibitors' aromatic moieties bound to the PAS region of *m*AChE, in accordance with our design hypothesis. Numerous face-to-face and edge-to-face aromatic interactions were observed between the inhibitors and *m*AChE. Furthermore, all inhibitors formed an internal hydrogen bond between one of the sulfonamide oxygens and the tertiary amine (Figure 3a and b) with an average heavy atom distance of 3.1 Å (SD 0.1 Å)⁴⁸. The interaction patterns in the CAS were similar in all seven structures, and consisted of electrostatic interactions, hydrogen bonds and van der Waal contacts. The inhibitors' diethyl-amine moieties presumably interact with Trp86 *via* hydrogen bonds of the NC–H...arene type, where the average distance of the closest carbon to the six-membered ring centroid of Trp86 was 3.8 Å (SD 0.1 Å).⁴⁸ Other interactions shared by the majority of the inhibitors in the CAS included contacts between the inhibitors' *N*-ethyl groups and Tyr337, Gly120, Gly121, Glu202 and His477. The following paragraphs will include a brief analysis of the inhibitors' interactions with the PAS region of AChE.

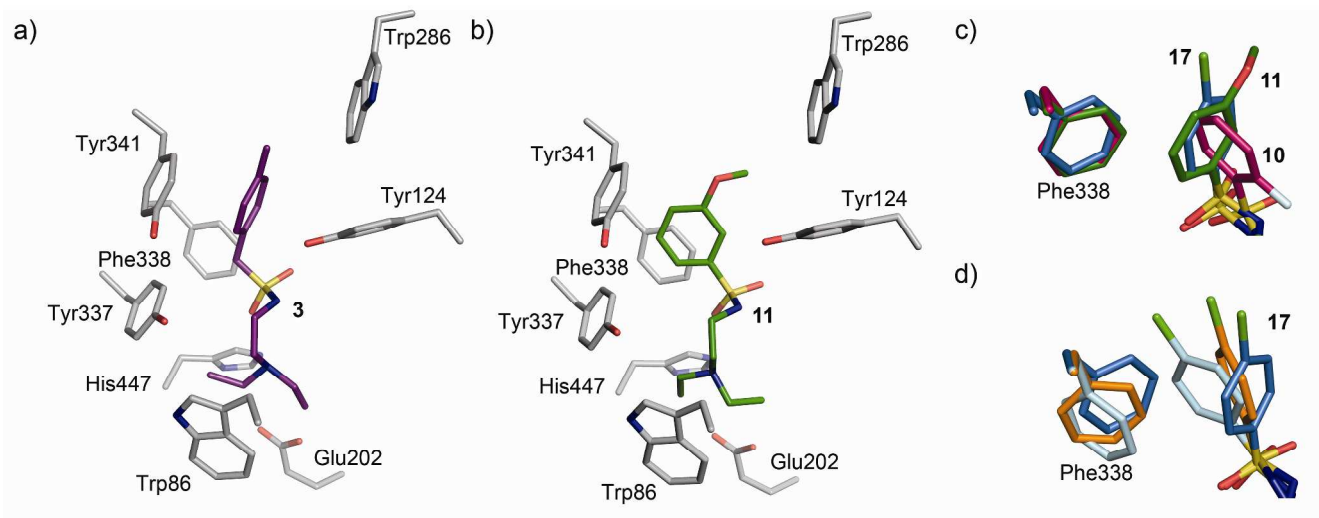


Figure 3. Crystal structures of *m*AChE•inhibitor complexes with *m*AChE residues in gray and (a) the benzylic inhibitor **3** (purple), and (b) the non-benzylic inhibitor **11** (green). (c) The PAS binding mode of the non-benzylic inhibitors **17** (dark blue), **11** (green), and **10** (pink) and residue Phe338 from the

1 respective complexes in the same coloring. (d) The multiple conformers with similar occupancy of
2 inhibitor **17** and Phe338 as seen in chain A (inhibitor conformers A and B marked in dark- and light
3 blue, respectively) and chain B (marked in orange).
4
5
6
7
8
9

10 **Benzylic inhibitors display a conserved binding conformation.** The benzylic inhibitors are
11 coordinated in the PAS in nearly identical conformations, which is exemplified by inhibitor **3** in Figure
12 3a. The inhibitors' aromatic rings were located between Tyr341 and Tyr124 allowing parallel-displaced
13 face-to-face interactions with Tyr341 with an average phenyl centroid–centroid distance of 4.2 Å (SD
14 0.1 Å).⁴⁸ The *para*-substituent and benzyl carbon of the inhibitor and the hydroxyl of Tyr341 were
15 oriented in a 90° angle with respect to each other, which is a preferred orientation in these stacking
16 interactions.⁴⁹ In addition, the benzylic inhibitors interacted with Tyr124 via O–H···arene type bonds
17 (phenyl centroid–oxygen distance of 3.1 Å (SD 0.1 Å)).⁴⁸ In comparison with other compounds binding
18 to AChE, the benzylic inhibitors form similar interactions with Tyr341 as the pyridinium oxime moiety
19 of HI-6. This interaction is, however, not observed in the complex with donepezil. Unlike our inhibitors,
20 both donepezil and HI-6 form aromatic interactions with Trp286, a residue in the PAS of AChE that
21 commonly participates in key interactions to many AChE inhibitors. For further details regarding key
22 protein-ligand interactions, and structural comparisons to HI-6 and donepezil, see the Supporting
23 Information. The most potent benzylic inhibitors included in this study all contain a *para*-substituent (**5**,
24 **6**, **7** and **8**). The increased potency can, on a structural basis, be interpreted as an effect from a
25 combination of increased van der Waals interactions (halogen–arene interactions),⁵⁰ and beneficial
26 dipole–dipole interactions with Tyr341, and in particular with Trp286. A similar case involving *para*-
27 chloro-substituted ligands of the serine protease factor Xa revealed the same trend as observed here; a
28 chlorine substituent resulted in more potent inhibitors compared to fluorine and methyl, which was
29 shown to be due to interactions with a tryptophan.⁵¹
30
31
32
33
34
35
36
37
38
39
40
41
42
43
44
45
46
47
48
49
50
51
52
53
54
55
56
57
58
59
60

Divergent binding conformations of the non-benzylic inhibitors. The non-benzylic inhibitors displayed three different binding modes depending on the arene substitution pattern, and these are shown in Figures 3b and 3c. The *meta*-substituted compounds **11** and **12** (exemplified by **11** in Figure 3b) participated in edge-to-face aromatic interactions with Tyr341 and in face-to-face (parallel-displaced) interactions with Phe338 (phenyl centroid–centroid distance 4.6 Å, SD 0.3 Å).⁴⁸ Overall, the most potent non-benzylic *meta*-substituted inhibitors **11** and **12** had a higher number of favorable interactions with PAS compared to the *para*- and *ortho*-substituted ones. In comparison to the binding mode of donepezil, **11** and **12** have ring conformations in a different plane compared to the dimethoxyindanone moiety of donepezil, thus interacting with other aromatic sites in PAS (*e.g.* Phe338). They also lack the stacking interaction donepezil has with Trp286.

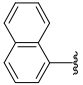
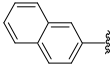
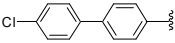
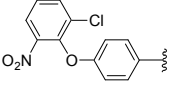
Interestingly, three different substituent-dependent conformations of the PAS-binding moieties of the non-benzylic inhibitors were observed (Figure 3c). The *meta*-substituted **11** and **12** had the same phenyl conformation, while two alternative conformations were observed for *ortho*-substituted **10** and the low affinity *para*-substituted **17**, respectively, where the ring was rotated 90° in the former and highly mobile in the latter (Figure 3c and 3d). The *ortho*-substituted **10** only participated in edge-to-face aromatic interactions with Tyr341. For compounds **11** and **12**, however, the *meta*-substituents formed contacts to Trp286 in addition to the edge-to-face interaction with Trp341. The pyridinium moiety of the reactivator HI-6 that stacks with Tyr341 has a similar orientation as the *ortho*-substituted **10**, and consequently a different orientation compared to the *meta*- and *para*-substituted non-benzylic inhibitors. The deviant binding mode of the *ortho*-substituted **10** was most likely a result of the rotational restriction imposed by the fluorine atom due to its proximity to the sulfonamide oxygens. Notably, the fluorine in its present position may form a hydrogen bond to the sulfonamide nitrogen with a heavy atom distance of 2.45 Å. This is most likely the preferred orientation over the significantly less occupied conformation (visible in chain A in the *m*AChE•**10** complex), where the ring is rotated 180 degrees around the phenyl-sulfur bond.

Para-chloro-substituted **17** displayed three different conformations in the PAS (two in chain A and one in Chain B), and as a consequence Phe338 displayed an assembly of different conformations (Figure 3d). Modeling of the dominating conformers of **17** and Phe338 suggests that the structural changes result in a stacking interaction (chain A) or edge-to-face interaction (chain B) between the inhibitor and *m*AChE. The conformational changes observed for **17** appear to be energetically unfavorable, which might explain the lower potency. The loss of potency of *para*-substituted compounds compared to the *meta*-substituted may be because a *para*-substituent, such as chlorine in **17**, would result in a clash with the side chain of Tyr341 if compound **17** would adopt the binding conformation displayed by the *meta*-substituted compounds.

Investigation of a second generation non-benzylic inhibitors with bicyclic aromatic systems. The binding of the non-benzylic compounds to AChE were shown to have beneficial entropies and the compounds displayed a range of binding modes in the PAS region. Increasing the number of interaction points between the inhibitor and AChE, and especially arene-stacking with Trp286, was deemed a reasonable strategy in the development of new inhibitors and reactivators leads. Hence, a second generation of non-benzylic compounds was synthesized to investigate the level of modifications needed to increase potency and alter the binding mode to AChE, and thereby to go beyond the previously established SAR. Four new molecules (set 2), all containing a bicyclic aromatic system in the PAS-binding moiety, were therefore synthesized using the same strategy as the previous analogues (Scheme 1), and were evaluated for inhibition of *m*AChE enzymatic activity (Table 2) on two separate occasions (see the Supporting Information). The naphthalene compound **21**, extended with an additional ring in positions corresponding to *ortho*-/*meta* to the sulfonamide, was clearly more potent than compound **22** with the additional phenyl in positions corresponding to *para*-/*meta*. Hence, these two compounds seem to adhere to the previously established SAR, showing that a *para*-substituent is detrimental to potency. Extending with *para*-chloro benzene (**23**) in the *para*-position also diminished the inhibition of AChE, suggesting that the SAR holds for this class of compounds as well. Interestingly, extending the PAS-

binding benzene with an additional phenyl (*i.e.*, 2-chloro-6-nitro-benzene, **24**) linked with an ether-bridge proved to be the most potent compound with an IC_{50} of 2.5 μM , *i.e.*, three times more potent than the most potent non-benzylic compound **11** in set 1. Notably, the *para*-methoxy **14** displayed an IC_{50} of only 119 μM , indicating that **24** does not seem to adhere to the SAR established for the non-benzylic compounds, which might indicate a different binding mode of inhibitor **24**.

Table 2. Inhibition of *m*AChE hydrolysis activity of compounds in set 2.

ID	R	Bioreplicate C ₁	
		IC_{50} (μM)	95% CI (μM) ^a
21		44	32-58
22		>700	-
23		>700	-
24		2.5	2.3-2.8

^a 95% confidence interval calculated from at least four replicates.

Crystallographic investigation of the most potent inhibitor. The crystal structure of *m*AChE in complex with **24** was determined at 2.5 Å resolution (for details, see the Supporting Information). The crystal structure showed that aromatic moieties of **24** bound in the PAS region of AChE but with a slightly different conformation, and that the diethyl amine bound in the CAS region with similar binding mode, compared to the previous inhibitors, as exemplified by an overlay with the *meta*-methoxy substituted **11** (Figure 4a). Only one conformation was observed for the adjacent amino acids and inhibitor **24**, as opposed to the *para*-substituted non-benzylic compound **17** which displayed multiple conformations (Figure 3d). Compared to compound **11**, compound **24** also stack with Phe338 (Figure

4b), but is shifted slightly deeper down in the gorge thereby allowing the 2-chloro-6-nitrophenol of **24** to form an additional face-to-face stacking interaction with Trp286 (benzene centroid–centroid distance 4.1 Å,⁴⁸ Figure 4b) in a similar conformation as the one observed for the dimethoxy-indanone moiety of donepezil. This key interaction with Trp286 most likely explains the higher potency of this inhibitor. Another potential key interaction is formed between the nitro group of **24** and the backbone nitrogen of Phe295 (Figure 4b), with a heavy atom distance of 3.3 Å.⁴⁸ Hydrogen bonds to this residue have previously been observed in several structures.^{25, 29, 42, 47}

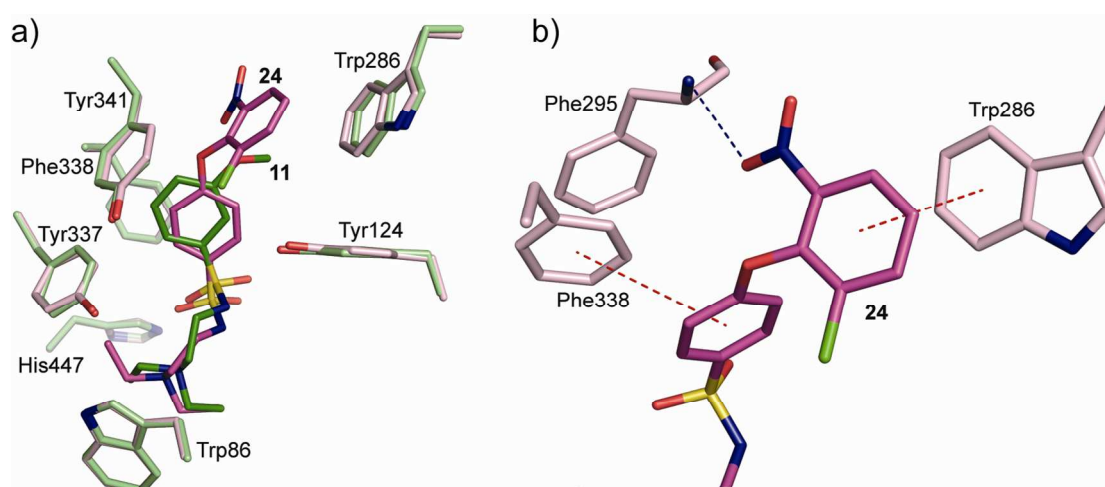


Figure 4. Crystal structures of (a) the superposed *mAChE*•inhibitor complexes with the non-benzylic inhibitors **11** (green) and **24** (pink), and (b) inhibitor **24** and PAS residues of *mAChE*

CONCLUSIONS

We have investigated the molecular interactions between AChE and two structurally similar classes of compounds and we could show that the two classes displayed different SARs, binding modes, and thermodynamic profiles when binding to AChE. Variations of the compound arene-substituents affected the compounds' steric, electrostatic, and van der Waals properties, which in turn affected the compounds' potency, confirming the importance of aromatic interactions in PAS also shown by others.^{23-24, 27, 35-38} Our data based on *both* biochemical and structural data revealed that the SARs in the

PAS of AChE are intricate; relatively small changes in the aromatic rings of the inhibitors can have striking effects on the binding modes, which implies that inhibitor design strategies based solely on SAR-conclusions are insufficient. Our results indicate that larger van der Waals contacts have a greater influence on aromatic interactions than different electronic distributions in the phenyl rings. For the benzylic compounds, a larger electron-withdrawing substituent in the *para*-position of the benzylic compounds was beneficial. For the non-benzylic compounds, a *meta*-substituent led to increased potency, a *para*-substituent led to decreased potency, while an *ortho*-substituent led to decreased potency and alternative binding modes. Analysis of ITC data showed that the two structurally similar series of inhibitors displayed a difference in the thermodynamic profiles, where the binding of the benzylic inhibitors to AChE was more enthalpy-driven compared to the non-benzylic inhibitors. The more entropy-driven non-benzylic compound class was investigated with a second generation of compounds. Inhibitor **24** in the second set proved to be the most potent inhibitor, and extended beyond the previously established SAR for the non-benzylic compounds. An additional ether-linked aromatic ring in the *para*-position increased the potency, which again is a reminder of the intricacy of SAR in AChE.

Taken together, we have utilized information from kinetic, crystallographic and thermodynamic data to establish detailed SARs specific for two structurally similar compound classes. The established SARs can be utilized in both inhibitor and reactivator design, focusing on fine-tuning the aromatic interactions in the PAS of AChE. We intend to extend the established divergent SARs of the compound classes investigated here to also include nerve agent inhibited *h*AChE,²⁸ and use the results to develop new reactivators. We believe that a good understanding of the intricate SARs of the PAS-binding moiety is critical in order to optimize the efficacy of reactivators while reducing the inhibition of the active AChE. Our design strategy will be to combine PAS-binding moieties with divergent SARs with sets of flexible CAS-binding moiety with reactivating properties to generate a tailored set of compounds for biochemically and structurally evaluation of free and nerve agent inhibited *h*AChE.

EXPERIMENTAL SECTION

Chemistry. Thin layer chromatography was performed on Merck precoated Silica-gel 60F254 plates with detection by ultra violet (UV)-light and staining with ninhydrin (0.75 g ninhydrin, 250 mL 95% EtOH, 2.5 mL glacial acetic acid) for detection of amines. Flash column chromatography was performed on silica gel (grade 9385, pore size 60 Å, 230-400 mesh) and eluent ethyl acetate/methanol 3:1. Preparative reversed-phased HPLC was performed on a prep-scale HPLC pump (flowrate 20 mL/min), a 151 UV/VIS detector (detection at 214 nm), and a VP 250/21 Nucleodor (C₁₈ HTec, 5 µm) column using a water/acetonitrile eluent system. Analytical reversed-phased HPLC for compounds **2-20** was performed on a Gilson® 322 HPLC pump (flowrate 1 mL/min), a Gilson® 172 diode array detector (detection at 210-360 nm), a Sedere Sedex 85 low-temperature evaporative light-scattering detector (ELSD), and an EC 150/4.6 Nucleodor (C₁₈ HTec, 5 µm) column using a water/acetonitrile/formic acid (0.005%) eluent system. Analytical reversed-phased HPLC for **21-24** was performed on a Shimadzu® LC-30AD pump (flowrate 1 mL/min) a Shimadzu SPD-M20A diode array detector (detection at 210-360nm) an EC 150/4.6 Nucleodor (C₁₈ HTec, 5 µm) column using a water/acetonitrile/formic acid (0.005%) eluent system. ¹H and ¹³C NMR spectra were recorded on a Bruker DRX-400 instrument in CDCl₃ [residual CHCl₃ (δH 7.26 ppm, δC 77.16 ppm)], CD₃OD [residual CH₃OH (δH 3.31 ppm, δC 49.00 ppm)] or (CD₃)₂SO [residual (CH₃)₂SO (δH 2.50 ppm, δC 39.52 ppm)]. NMR spectra and HPLC chromatograms for all compounds are given in the Supporting Information. Purities of the biologically evaluated compounds were >95% determined by analytical HPLC.

General procedure for the synthesis of *N*-[2-(diethylamino)-ethyl]-benzenemethanesulfonamides and *N*-[2-(diethylamino)-ethyl]-benzenesulfonamides exemplified by *N*-[2-(diethylamino)ethyl]-3-methoxy-benzenesulfonamide (11**).** 3-Methoxybenzenesulfonyl chloride (0.103 g, 0.5 mmol) was suspended in CH₂Cl₂ (2.5 mL). The suspension was cooled to 0 °C, *N,N*-diethylethylenediamine (0.07g, 0.6 mmol) was added slowly over 10 min and the mixture was stirred at rt until the starting material was consumed (4 h). CH₂Cl₂ (2.5 mL) was added to the reaction flask and the organic phase

was washed once with NaHCO₃ (aq, satd, 2.0 mL). The organic phase was dried over anhydrous Na₂SO₄ and removed under reduced pressure. Purified by flash chromatography (ethyl acetate/methanol 3:1) gave the product in 89% yield. HPLC purity: > 95%.

***N*-[2-(Diethylamino)ethyl]-1-phenyl-methanesulfonamide (2).** Yield 55%. Purified by preparative HPLC. ¹H NMR (CD₃OD): δ 1.02 (t, 6H, *J*=7.3 Hz), 2.46-2.57 (m, 6H), 2.95-3.01 (m, 2H), 4.34 (s, 2H), 7.30-7.46 (m, 5H). ¹³C NMR (CD₃OD): δ 11.54, 41.76, 48.10, 53.97, 59.33, 129.48, 129.62, 131.49, 131.98.

***N*-[2-(Diethylamino)ethyl]-1-(4-methylphenyl)methanesulfonamide (3).** Yield 35%. ¹H NMR (CD₃OD): δ 1.02 (t, 6H, *J*=7.2 Hz), 2.34 (s, 3H), 2.48-2.57 (m, 6H), 2.93-2.99 (m, 2H), 4.29 (s, 2H), 7.16-7.22 (m, 2H), 7.27-7.34 (m, 2H). ¹³C NMR (CD₃OD): δ 11.50, 21.20, 41.76, 48.13, 53.94, 59.09, 128.35, 130.25, 131.85, 139.53.

***N*-[2-(Diethylamino)ethyl]-1-(4-fluorophenyl)-methanesulfonamide (4).** Yield 69%. Purified by flash chromatography. ¹H NMR (CDCl₃): δ 0.92 (t, 6H, *J*=7.1 Hz), 2.40-2.49 (m, 6H), 2.93 (t, 2H, *J*=5.9 Hz), 4.20 (s, 2H), 5.01 (br s, 1H), 6.99-7.06 (m, 2H), 7.33-7.39 (m, 2H). ¹³C NMR (CDCl₃): δ 11.59, 40.90, 46.37, 51.98, 57.78, 115.71 (d, 2C, *J*=21.8 Hz), 125.57 (d, 1C, *J*=2.9 Hz), 132.38 (d, 2C, *J*=8.0 Hz), 162.91 (d, 1C, *J*=248.0 Hz).

1-(4-Chlorophenyl)-*N*-[2-(diethylamino)ethyl]methanesulfonamide (5). Yield 61%. ¹H NMR (CD₃OD): δ 1.03 (t, 6H, *J*=7.1 Hz), 2.49-2.58 (m, 6H), 2.99-3.04 (m, 2H), 4.34 (s, 2H), 7.37-7.45 (m, 4H). ¹³C NMR (CD₃OD): δ 11.53, 41.75, 48.12, 53.98, 58.46, 129.70, 130.39, 133.53, 135.55.

***N*-(2-Diethylamino-ethyl)-*C*-(4-trifluoromethyl-phenyl)-methanesulfonamide (6).** Yield 82%. Purified by flash chromatography. ¹H NMR (CDCl₃): δ 0.92 (t, 6H, *J*=7.1 Hz), 7.37-7.50 (m, 6H), 2.97 (t, 2H, *J*=5.9 Hz), 4.29 (s, 2H), 5.10 (br s, 1H), 7.46-7.63 (m, 4H). ¹³C NMR (CDCl₃): δ 11.54, 40.88, 46.41, 51.95, 58.16, 123.96 (q, 1C, *J*=272.0 Hz), 125.39-125.76 (m, 2C), 130.70 (q, 1C, *J*=32.4 Hz), 131.07, 133.77.

***C*-(4-Bromo-phenyl)-*N*-(2-diethylamino-ethyl)-methanesulfonamide (7).** Yield 94%. Purified by flash chromatography. ¹H NMR (CDCl₃): δ 0.97 (t, 6H, *J*=7.1 Hz), 2.44-2.53 (m, 6H), 2.98 (t, 2H, *J*=5.9

Hz), 4.22 (s, 2H), 5.15 (br s, 1H), 7.27-7.53 (m, 4H). ^{13}C NMR (CDCl_3): δ 11.57, 40.84, 46.39, 51.95, 57.93, 122.84, 128.66, 131.81, 132.22.

1-(3,4-Dichlorophenyl)-N-[2-(diethylamino)ethyl]-methanesulfonamide (8). Yield 59%. ^1H NMR (CD_3OD): δ 1.04 (t, 6H, $J=7.2$ Hz), 2.50-2.60 (m, 6H), 3.02-3.08 (m, 2H), 4.36 (s, 2H), 7.34-7.40 (m, 1H), 7.52-7.57 (m, 1H), 7.60-7.65 (m, 1H). ^{13}C NMR (CD_3OD): δ 11.51, 41.76, 48.11, 53.97, 57.90, 131.65, 131.78, 132.44, 133.36, 133.54, 133.87.

N-[2-(Diethylamino)ethyl]-benzenesulfonamide (9). Yield 95%. Purified by flash chromatography. ^1H NMR (CDCl_3): δ 0.89 (t, 6H, $J=7.1$ Hz), 2.35 (q, 4H, $J=7.0$ Hz), 2.45 (t, 2H, $J=5.7$ Hz), 2.94 (t, 2H, $J=5.8$ Hz), 7.49-7.60 (m, 3H), 7.85-7.89 (m, 2H). ^{13}C NMR (CDCl_3): δ 11.77, 40.32, 46.34, 51.02, 127.23, 129.15, 132.66, 139.82.

N-[2-(Diethylamino)ethyl]-2-fluoranyl-benzenesulfonamide (10). Yield 42%. ^1H NMR (CD_3OD): δ 0.98 (t, 6H, $J=7.2$ Hz), 2.45-2.58 (m, 6H), 3.00-3.06 (m, 2H), 7.28-7.39 (m, 2H), 7.63-7.70 (m, 1H), 7.85-7.91 (m, 1H). ^{13}C NMR (CD_3OD): δ 11.52, 41.33, 48.02, 53.04, 118.10 (d, 1C, $J=21.7$ Hz), 125.70 (d, 1C, $J=3.7$ Hz), 129.80 (d, 1C, $J=13.8$ Hz), 131.22, 136.27 (d, 1C, $J=8.4$ Hz), 160.24 (d, 1C, $J=254.0$ Hz).

N-[2-(Diethylamino)ethyl]-3-methoxy-benzenesulfonamide (11). Yield 89%. Purified by flash chromatography. ^1H NMR (CDCl_3): δ 0.86 (t, 6H, $J=7.1$ Hz), 2.32 (q, 4H, $J=7.1$ Hz), 2.42 (t, 2H, $J=5.9$ Hz), 2.91 (t, 2H, $J=5.9$ Hz), 3.80 (s, 3H), 5.38 (br s, 1H), 7.02-7.08 (m, 1H), 7.32-7.43 (m, 3H). ^{13}C NMR (CDCl_3): δ 11.61, 40.27, 46.26, 50.94, 55.65, 111.84, 118.88, 119.19, 130.09, 140.79, 159.94.

N-[2-(Diethylamino)ethyl]-3-(trifluoromethyl)benzenesulfonamide (12). Yield 96%. Purified by flash chromatography. ^1H NMR (CDCl_3): δ 0.86 (t, 6H, $J=7.1$ Hz), 2.34 (q, 4H, $J=7.1$ Hz), 2.46 (t, 2H, $J=5.8$ Hz), 2.94 (t, 2H, $J=5.8$ Hz), 5.54 (br s, 1H), 7.65 (t, 1H, $J=7.8$ Hz), 7.81 (d, 1H, $J=7.6$ Hz), 8.05 (d, 1H, $J=7.8$ Hz), 8.11 (s, 1H). ^{13}C NMR (CDCl_3): δ 11.57, 40.30, 46.32, 50.93, 123.29 (q, 1C, $J=272.4$ Hz), 124.12 (d, 1C, $J=3.6$ Hz), 129.21 (d, 1C, $J=3.3$ Hz), 129.95, 130.43, 131.77 (q, 1C, $J=33.3$ Hz), 141.20.

3-Chloro-*N*-(2-diethylamino-ethyl)-benzenesulfonamide (13). Yield 23%. ^1H NMR (CD_3OD): δ 1.01 (t, 6H, $J=7.0$ Hz), 2.51-2.61 (m, 6H), 2.95-3.01 (m, 1H), 7.54-7.61 (m, 1H), 7.62-7.68 (m, 1H), 7.76-7.82 (m, 1H), 7.84-7.88 (m, 1H). ^{13}C NMR (CD_3OD): δ 11.31, 41.38, 48.11, 52.95, 126.39, 127.91, 131.96, 133.65, 136.19, 143.85.

***N*-[2-(Diethylamino)ethyl]-4-methoxy-benzenesulfonamide (14).** Yield 51%. Purified by preparative HPLC. ^1H NMR (CD_3OD): δ 0.99 (t, 6H, $J=7.2$ Hz), 2.46-2.58 (m, 6H), 2.87-2.97 (m, 2H), 3.87 (s, 3H), 7.08 (d, 2H, $J=8.9$ Hz), 7.79 (d, 2H, $J=8.9$ Hz). ^{13}C NMR (CD_3OD): δ 11.40, 41.32, 48.08, 52.90, 56.20, 115.34, 130.19, 133.15, 164.48.

***N*-[2-(Diethylamino)ethyl]-4-methyl-benzenesulfonamide (15).** Yield 80%. ^1H NMR (CD_3OD): δ 0.98 (t, 6H, $J=7.2$ Hz), 2.43 (s, 3H), 2.45-2.55 (m, 6H), 2.92 (m, 2H), 7.38 (d, 2H, $J=7.9$ Hz), 7.74 (d, 2H, $J=7.9$ Hz). ^{13}C NMR (CD_3OD): δ 11.49, 21.43, 41.42, 48.03, 52.93, 128.07, 130.74, 138.80, 144.72.

***N*-[2-(Diethylamino)ethyl]-4-fluoranyl-benzenesulfonamide (16).** Yield 81%. ^1H NMR (CD_3OD): δ 0.98 (t, 6H, $J=7.2$ Hz), 2.45-2.57 (m, 6H), 2.92-2.98 (m, 2H), 7.28-7.25 (m, 2H), 7.88-7.95 (m, 2H). ^{13}C NMR (CD_3OD): δ 11.50, 41.49, 48.04, 53.00, 117.23 (d, 2C, $J=22.8$ Hz), 130.94 (d, 2C, $J=9.4$ Hz), 138.16 (d, 1C $J=3.0$ Hz), 166.38 (d, 1C, $J=251.6$ Hz).

4-Chloranyl-*N*-[2-(diethylamino)ethyl]benzenesulfonamide (17). Yield 59%. ^1H NMR (CD_3OD): δ 0.99 (t, 6H, $J=7.2$ Hz), 2.46-2.58 (m, 6H), 2.92-2.99 (m, 2H), 7.56-7.61 (m, 2H), 7.80-7.87 (m, 2H). ^{13}C NMR (CD_3OD): δ 11.46, 41.46, 48.05, 53.01, 129.75, 130.45, 139.82, 140.69.

***N*-[2-(Diethylamino)ethyl]-4-nitro-benzenesulfonamide (18).** Yield 80%. ^1H NMR (CD_3OD): δ 1.01 (t, 6H, $J=7.2$ Hz), 2.50-2.61 (m, 6H), 3.00-3.06 (m, 2H), 8.08-8.14 (m, 2H), 8.40-8.46 (m, 2H). ^{13}C NMR (CD_3OD): δ 11.49, 41.59, 48.04, 53.18, 125.42, 129.41, 147.85, 151.45.

4-Chloranyl-*N*-[2-(diethylamino)ethyl]-2-fluoranyl-benzenesulfonamide (19). Yield 50%. ^1H NMR (CD_3OD): δ 1.02 (t, 6H, $J=7.2$ Hz), 2.49-2.63 (m, 6H), 3.03-3.10 (m, 2H), 7.39-7.45 (m, 1H), 7.46-7.52 (m, 1H), 7.88 (t, 1H, $J=8.3$ Hz). ^{13}C NMR (CD_3OD): δ 11.48, 41.33, 48.05, 53.14, 118.86 (d,

1C, $J=25.0$ Hz), 126.13 (d, 1C, $J=3.6$ Hz), 128.98 (d, 1C, $J=14.5$ Hz), 132.37, 141.21 (d, 1C, $J=9.6$ Hz), 160.14 (d, 1C, $J=257.8$ Hz).

***N*-[2-(Diethylamino)ethyl]-3,4-difluoranyl-benzenesulfonamide (20).** Yield 60%. ^1H NMR (CD_3OD): δ 1.01 (t, 6H, $J=7.2$ Hz), 2.50-2.60 (m, 6H), 2.96-3.01 (m, 2H), 7.45-7.54 (m, 1H), 7.67-7.74 (m, 1H), 7.75-7.83 (m, 1H). ^{13}C NMR (CD_3OD): δ 11.38, 41.44, 48.06, 53.01, 117.86 (d, 1C, $J=20.00$ Hz), 119.43 (d, 1C, $J=18.80$ Hz), 125.40-125.80 (m, 1C), 139.02-139.37 (m, 1C), 151.48 (dd, 1C, $J=13.9$, 271.90 Hz), 154.00 (dd, 13.9, 276.5 Hz).

Naphtalene-1-sulfonic acid (2-diethylamino-ethyl)-amide (21) Yield 64%. Purified by flash chromatography. ^1H NMR (CDCl_3): δ 0.75 (t, 6H, $J=7.2$ Hz), 2.19 (q, 4H, $J=7.1$ Hz), 2.34 (t, 2H, $J=5.9$ Hz), 2.85 (t, 2H, $J=5.8$ Hz), 7.54 (t, 1H, $J=7.7$ Hz), 7.57-7.62 (m, 1H), 7.65-7.70 (m, 1H), 7.94 (d, 1H, $J=8.4$ Hz), 7.94 (d, 1H, $J=8.4$ Hz), 8.27 (d, 1H, $J=7.4$ Hz), 8.67 (d, 1H, $J=8.6$ Hz). ^{13}C NMR (CDCl_3): δ 11.34, 40.27, 45.85, 50.88, 124.06, 124.43, 126.80, 128.20, 128.26, 129.03, 129.71, 134.05, 134.22.

Naphtalene-2-sulfonic acid (2-diethylamino-ethyl)-amide (22). Yield 25%. Purified by Flash chromatography. ^1H NMR (CDCl_3): δ 0.89 (t, 6H $J=7.1$ Hz), 2.35 (q, 4H, $J=7.1$ Hz), 2.47 (t, 2H, $J=5.7$ Hz), 2.94-3.00 (m, 2H), 7.58-7.68 (m, 2H), 7.82-7.86 (m, 1H), 7.89-7.93 (m, 1H), 7.94-7.99 (m, 2H), 8.41-8.46 (m, 1H). ^{13}C NMR (CDCl_3): δ 11.68, 40.26, 46.33, 51.10, 122.53, 127.66, 128.04, 128.63, 128.83, 129.34, 129.54, 132.27, 134.90, 136.56.

4'-Chloro-biphenyl-4-sulfonic acid (2-diethylamino-ethyl)-amide (23) Yield 9%. Purified by flash chromatography. ^1H NMR (CDCl_3): δ 1.02 (t, 6H $J=7.1$ Hz), 2.56 (q, 4H, $J=7.2$ Hz), 2.63-2.69 (m, 2H), 3.06-3.12 (m, 2H), 7.41-7.48 (m, 2H), 7.50-7.56 (m, 2H), 7.64-7.71 (m, 2H), 7.91-7.98 (m, 2H). ^{13}C NMR (CDCl_3): δ 11.06, 39.94, 46.85, 51.74, 127.65, 127.85, 128.67, 129.37, 134.86, 137.88, 138.80, 144.34.

4-(2-Chloro-6-nitro-phenoxy)-*N*-(2-diethylamino-ethyl)-benzenesulfonamide (24). Yield 87%. Purified by HPLC. ^1H NMR ($(\text{CD}_3)_2\text{SO}$): δ 0.87 (t, 6H, $J=7.2$ Hz), 2.34-2.45 (m, 6H), 2.76-2.86 (m, 2H), 7.06-7.14 (m, 2H), 7.47 (bs, 1H), 7.64 (t, 1H, $J=8.3$ Hz), 7.76-7.82 (m, 2H), 8.05-8.12 (m, 1H),

8.15-8.21 (m, 2H). ^{13}C NMR ((CD_3) $_2\text{SO}$): δ 11.41, 40.71, 46.49, 51.45, 115.59, 125.05, 127.97, 129.02, 129.13, 135.22, 136.05, 142.23, 144.27, 159.09, 163.33.

Determination of the half-maximal inhibitory concentration (IC_{50}). Compound stock solutions were prepared by dissolving compounds (1-6 mg) in dimethyl sulfoxide (DMSO) to a final concentration of 0.1 M, and stocks were prepared fresh prior to each IC_{50} -determination. Two batches of recombinant *m*AChE were independently expressed and purified as previously described.⁵² Batch A was immediately used for determination of IC_{50} -values (bioreplicate A), whereas batch B was stored on ice for three years prior to use (bioreplicate B).⁵³ A third stock of AChE was used for IC_{50} determinations of compounds **21-24** termed bioreplicate C. All stock solutions and buffers were independently prepared for determination of the two bioreplicates. The enzymatic activity was measured using the Ellman assay⁴³ at a wavelength of 412 nm and a temperature of 30 °C. The IC_{50} -values were obtained by determining the enzymatic activity in the presence of various concentrations of the inhibitors using a buffer composed of 0.2 mM 5,5'-dithiobis-(2-nitrobenzoic acid), 1 mM acetylthiocholine iodide and 0.1 M phosphate buffer pH 8.0. The final assay volume was 200 μL and the enzymatic reaction was followed during 120 seconds using a BioTek Power Wave plate reader. At least four replicate IC_{50} determinations were performed for each experiment. The obtained dose-response curve was analyzed using the Enzyme Kinetics module of Graph Pad Prism version 5.03. The dose-response curves was fitted using the log(inhibitor) vs. response variable slope (four parameters) equation.

Isothermal titration calorimetry. All buffers were degassed and sterile filtered prior to use. Compound- and *m*AChE concentrations were prepared in phosphate buffer 0.1 M, pH 7.4 as follows: **5** 1.60 mM, *m*AChE 0.12 mM; **6**, 2.50 mM, *m*AChE 0.17 mM; **12**, 3.00 mM, *m*AChE 0.20 mM; and **13**, 2.80 mM, *m*AChE, 0.15 mM. The ITC experiments were performed at 25.0 °C (26 °C for **13**) on an ITC200 instrument (MicroCalTM, GE Healthcare Life Sciences). The protein- and compound solutions (concentrations above) were loaded into the reaction cell and syringe, respectively, and 35 automated injections of 1.11 μL each with a 250 s break in between each injection were made. The stirring speed was 600 rpm. A reference run was performed for each experiment where compound was injected into

pure buffer under the same conditions as for the main experiment. The injection heat peaks were automatically integrated, the heat peaks from the reference experiment were subtracted, and the data was analyzed using the single-site binding model, with 300 iterations of the Chi-Sqr fitting routine in Origin SR4 software.⁵⁴

Crystallographic data collection and structure refinement. *mAChE* was crystallized as previously described.⁵⁵ In short, crystals were grown at a protein concentration of 10 mg/mL with well solutions composed of 27–31 % (w/v) polyethylene glycol mono-methyl ether 750 and 100 mM HEPES, pH 7.0–7.1. Drop sizes were 2 μ L at a ratio of 1:1 of the protein and the mother liquid. The compounds presented in this study were soaked into *mAChE* crystals prior to flash-freezing in liquid nitrogen for data collection as previously described.⁴² X-ray diffraction data were collected at the MAX-lab synchrotron (Lund, Sweden), on beamlines I911-2 and I911-3 equipped with MAR Research CCD detectors. The images were collected at an oscillation range of 1° per exposure. The intensity data were indexed and integrated using XDS⁵⁶ and scaled using Scala.⁵⁷ The structures were determined by rigid-body refinement with a modified *apo* structure of *mAChE* (PDB entry code 1J06)⁸ as a starting model. Further crystallographic refinement was performed using the Phenix software suite.⁵⁸ Several rounds of refinement were performed, alternating with manual rebuilding in COOT.⁵⁹ The quality of the final models were validated using WHATCHECK⁶⁰ and the figures were constructed using PyMol.⁶¹ The crystallographic statistics are listed in the Supporting Information. The coordinates and structure factors of each *mAChE*•ligand complex structure have been deposited in the RCSB Protein Data Bank (www.pdb.org) with accession codes 4B7Z, 4B80, 4B81, 4B82, 4B83, 4B84, 4B85, and 4BTL for *mAChE*•**3**, *mAChE*•**4**, *mAChE*•**5**, *mAChE*•**10**, *mAChE*•**11**, *mAChE*•**12** and *mAChE*•**17**, and *mAChE*•**24**, respectively.

ASSOCIATED CONTENT

Supporting Information

Bioassay results of compound sets 1 and 2; ITC heat-diagrams and titration curve-fitting; crystallographic data collection and structure refinement; general description of the crystal structures and key protein-ligand interactions; structural comparisons of benzylic and non-benzylic inhibitors with donepezil and HI-6; ^1H and ^{13}C NMR-spectra; analytical HPLC spectra. This material is available free of charge via the Internet at <http://pubs.acs.org>.

PDB accession codes

4B7Z, 4B80, 4B81, 4B82, 4B83, 4B84, 4B85, 4BTL.

ACKNOWLEDGMENTS

AL thanks the Swedish Research Council and Umeå University for financial support and the authors thank the personnel at the MAXlab beam-lines for their excellent technical support.

AUTHOR INFORMATION

Corresponding Authors

FE: Phone: +46-90-106815; E-mail: fredrik.ekstrom@foi.se. AL: Phone: +46-90-7866890; E-mail: anna.linusson@chem.umu.se.

Notes

The authors declare no competing financial interest

ABBREVIATIONS USED

AChE, acetylcholinesterase; AD, Alzheimer's disease, *m*AChE, *mus musculus* acetylcholinesterase; PAS, peripheral anionic site; CAS, catalytic site; SAR, structure-activity relationship; ITC, isothermal titration calorimetry; IC_{50} , half-maximal inhibitory concentration; K_d dissociation constant; HTS, high-

throughput screening; ΔG , change in Gibbs free energy; ΔH , change in enthalpy; ΔS , change in entropy; K_d , dissociation constant; SD, standard deviation.

REFERENCES

- (1) Taylor, J. L.; Mayer, R. T.; Himel, C. M., Conformers of acetylcholinesterase - a mechanism of allosteric control. *Mol. Pharm.* **1994**, *45*, 74-83.
- (2) Holzgrabe, U.; Kapkova, P.; Alptuzun, V.; Scheiber, J.; Kugelmann, E., Targeting acetylcholinesterase to treat neurodegeneration. *Expert Opin. Ther. Tar.* **2007**, *11*, 161-179.
- (3) Perry, E. K.; Perry, R. H.; Blessed, G.; Tomlinson, B. E., Changes in brain cholinesterases in senile dementia of Alzheimer type. *Neuropath. Appl. Neuro.* **1978**, *4*, 273-277.
- (4) Talesa, V. N., Acetylcholinesterase in Alzheimer's disease. *Mech. Ageing Dev.* **2001**, *122*, 1961-1969.
- (5) Johannsen, P., Long-term cholinesterase inhibitor treatment of Alzheimer's disease. *CNS Drugs* **2004**, *18*, 757-768.
- (6) Jackson, S.; Ham, R. J.; Wilkinson, D., The safety and tolerability of donepezil in patients with Alzheimer's disease. *Brit. J. Clin. Pharmacol.* **2004**, *58*, 1-8.
- (7) de Koning, M. C.; Joosen, M. J. A.; Noort, D.; van Zuylen, A.; Tromp, M. C., Peripheral site ligand-oxime conjugates: a novel concept towards reactivation of nerve agent-inhibited human acetylcholinesterase. *Bioorg. Med. Chem.* **2011**, *19*, 588-594.
- (8) Bourne, Y.; Taylor, P.; Radić, Z.; Marchot, P., Structural insights into ligand interactions at the acetylcholinesterase peripheral anionic site. *Embo J.* **2003**, *22*, 1-12.
- (9) Sussman, J. L.; Harel, M.; Frolow, F.; Oefner, C.; Goldman, A.; Toker, L.; Silman, I., Atomic-structure of acetylcholinesterase from Torpedo-californica - a prototypic acetylcholine-binding protein. *Science* **1991**, *253*, 872-879.

- (10) Cheung, J.; Rudolph, M. J.; Burshteyn, F.; Cassidy, M. S.; Gary, E. N.; Love, J.; Franklin, M. C.; Height, J. J., Structures of human Acetylcholinesterase in complex with pharmacologically important ligands. *J. Med. Chem.* **2012**, *55*, 10282-10286.
- (11) Eskander, M. F.; Nagykerly, N. G.; Leung, E. Y.; Khelghati, B.; Geula, C., Rivastigmine is a potent inhibitor of acetyl- and butyrylcholinesterase in Alzheimer's plaques and tangles. *Brain Res.* **2005**, *1060*, 144-152.
- (12) Galdeano, C.; Viayna, E.; Arroyo, P.; Bidon-Chanal, A.; Blas, J. R.; Munoz-Torrero, D.; Luque, F. J., Structural determinants of the multifunctional profile of dual binding site acetylcholinesterase inhibitors as anti-Alzheimer agents. *Curr. Pharm. Des.* **2010**, *16*, 2818-2836.
- (13) Zhang, R. W.; Tang, X. C.; Han, Y. Y.; Sang, G. W.; Zhang, Y. D.; Ma, Y. X.; Zhang, C. L.; Yang, R. M., Drug-evaluation of huperzine-a in the treatment of senile memory disorders. *Acta Pharm. Sin.* **1991**, *12*, 250-252.
- (14) Wang, R.; Yan, H.; Tang, X. C., Progress in studies of huperzine A, a natural cholinesterase inhibitor from Chinese herbal medicine. *Acta Pharmacol. Sin.* **2006**, *27*, 1-26.
- (15) Radić, Z.; Taylor, P., Interaction kinetics of reversible inhibitors and substrates with acetylcholinesterase and its fasciculin 2 complex. *J. Biol. Chem.* **2001**, *276*, 4622-4633.
- (16) Carlier, P. R.; Han, Y. F.; Chow, E. S. H.; Li, C. P. L.; Wang, H.; Lieu, T. X.; Wong, H. S.; Pang, Y. P., Evaluation of short-tether bis-THA AChE inhibitors. A further test of the dual binding site hypothesis. *Bioorg. Med. Chem.* **1999**, *7*, 351-357.
- (17) Savini, L.; Campiani, G.; Gaeta, A.; Pellerano, C.; Fattorusso, C.; Chiasserini, L.; Fedorko, J. M.; Saxena, A., Novel and potent tacrine-related hetero- and homobivalent ligands for acetylcholinesterase and butyrylcholinesterase. *Bioorg. Med. Chem. Lett.* **2001**, *11*, 1779-1782.
- (18) Savini, L.; Gaeta, A.; Fattorusso, C.; Catalanotti, B.; Campiani, G.; Chiasserini, L.; Pellerano, C.; Novellino, E.; McKissic, D.; Saxena, A., Specific targeting of acetylcholinesterase and

- 1 butyrylcholinesterase recognition sites. Rational design of novel, selective, and highly potent
2 cholinesterase inhibitors. *J. Med. Chem.* **2003**, *46*, 1-4.
- 3
4
5 (19) Campiani, G.; Fattorusso, C.; Butini, S.; Gaeta, A.; Agnusdei, M.; Gemma, S.; Persico, M.;
6 Catalanotti, B.; Savini, L.; Nacci, V.; Novellino, E.; Holloway, H. W.; Greig, N. H.; Belinskaya,
7 T.; Fedorko, J. M.; Saxena, A., Development of molecular probes for the identification of extra
8 interaction sites in the mid-gorge and peripheral sites of butyrylcholinesterase (BuChE). Rational
9 design of novel, selective, and highly potent BuChE inhibitors. *J. Med. Chem.* **2005**, *48*, 1919-
10 1929.
- 11
12
13
14
15
16
17
18
19 (20) Rydberg, E. H.; Brumshtein, B.; Greenblatt, H. M.; Wong, D. M.; Shaya, D.; Williams, L. D.;
20 Carlier, P. R.; Pang, Y. P.; Silman, I.; Sussman, J. L., Complexes of alkylene-linked tacrine
21 dimers with *Torpedo californica* acetylcholinesterase: binding of bis(5)-tacrine produces a
22 dramatic rearrangement in the active-site gorge. *J. Med. Chem.* **2006**, *49*, 5491-5500.
- 23
24
25
26
27
28
29 (21) Lewis, W. G.; Green, L. G.; Grynszpan, F.; Radić, Z.; Carlier, P. R.; Taylor, P.; Finn, M. G.;
30 Sharpless, K. B., Click chemistry in situ: acetylcholinesterase as a reaction vessel for the
31 selective assembly of a femtomolar inhibitor from an array of building blocks. *Angew. Chem.*
32 *Int. Ed.* **2002**, *41*, 1053-1057.
- 33
34
35
36
37
38 (22) Bourne, Y.; Kolb, H. C.; Radić, Z.; Sharpless, K. B.; Taylor, P.; Marchot, P., Freeze-frame
39 inhibitor captures acetylcholinesterase in a unique conformation. *P. Natl. Acad. Sci. USA* **2004**,
40 *101*, 1449-1454.
- 41
42
43
44
45 (23) Villalobos, A.; Blake, J. F.; Biggers, C. K.; Butler, T. W.; Chapin, D. S.; Chen, Y. P. L.; Ives, J.
46 L.; Jones, S. B.; Liston, D. R.; Nagel, A. A.; Nason, D. M.; Nielsen, J. A.; Shalaby, I. A.; White,
47 W. F., Novel benzisoxazole derivatives as potent and selective inhibitors of acetylcholinesterase.
48 *J. Med. Chem.* **1994**, *37*, 2721-2734.
- 49
50
51
52
53
54
55 (24) Nagel, A. A.; Liston, D. R.; Jung, S.; Mahar, M.; Vincent, L. A.; Chapin, D.; Chen, Y. L.;
56 Hubbard, S.; Ives, J. L.; Jones, S. B.; Nielsen, J. A.; Ramirez, A.; Shalaby, I. A.; Villalobos, A.;
57 White, W. F., Design and synthesis of 1-Heteroaryl-3-(1-benzyl-4-piperidiny)propan-1-one
58
59
60

- derivatives as potent, selective acetylcholinesterase inhibitors. *J. Med. Chem.* **1995**, 38, 1084-1089.
- (25) Kryger, G.; Silman, I.; Sussman, J. L., Structure of acetylcholinesterase complexed with E2020 (Aricept (R)): implications for the design of new anti-Alzheimer drugs. *Structure* **1999**, 7, 297-307.
- (26) Sugimoto, H.; Yamanishi, Y.; Iimura, Y.; Kawakami, Y., Donepezil hydrochloride (E2020) and other acetylcholinesterase inhibitors. *Curr. Med. Chem.* **2000**, 7, 303-339.
- (27) Ishichi, Y.; Sasaki, M.; Setoh, M.; Tsukamoto, T.; Miwatashi, S.; Nagabukuro, H.; Okanishi, S.; Imai, S.; Saikawa, R.; Doi, T.; Ishihara, Y., Novel acetylcholinesterase inhibitor as increasing agent on rhythmic bladder contractions: SAR of 8-{3-[1-(3-fluorobenzyl)piperidin-4-yl]propanoyl}-1,2,5,6-tetrahydro-4H-pyrrolo[3,2,1-ij]quinolin-4-one (TAK-802) and related compounds. *Bioorg. Med. Chem.* **2005**, 13, 1901-1911.
- (28) Artursson, E.; Andersson, P. O.; Akfur, C.; Linusson, A.; Börjegen, S.; Ekström, F., Catalytic-site conformational equilibrium in nerve-agent adducts of acetylcholinesterase: Possible implications for the HI-6 antidote substrate specificity. *Biochem. Pharmacol.* **2013**, 85, 1389-1397.
- (29) Ekström, F.; Hörnberg, A.; Artursson, E.; Hammarström, L. G.; Schneider, G.; Pang, Y. P., Structure of HI-6 center dot sarin-Acetylcholinesterase determined by X-Ray crystallography and molecular dynamics simulation: reactivator mechanism and design. *PLoS One* **2009**, 4, e5957.
- (30) Kaur, J.; Zhang, M. Q., Molecular modelling and QSAR of reversible acetylcholinesterase inhibitors. *Curr. Med. Chem.* **2000**, 7, 273-294.
- (31) Bolognesi, M. L.; Minarini, A.; Tumiatti, V.; Melchiorre, C., Progress in acetylcholinesterase inhibitors for Alzheimer's disease. *Expert Opin. Ther. Pat.* **2006**, 16, 811-823.

- (32) Tumiatiti, V.; Bolognesi, M. L.; Minarini, A.; Rosini, M.; Milelli, A.; Matera, R.; Melchiorre, C., Progress in acetylcholinesterase inhibitors for Alzheimer's disease: an update. *Expert Opin. Ther. Pat.* **2008**, *18*, 387-401.
- (33) Saxena, A.; Fedorko, J. M.; Vinayaka, C. R.; Medhekar, R.; Radić, Z.; Taylor, P.; Lockridge, O.; Doctor, B. P., Aromatic amino-acid residues at the active and peripheral anionic sites control the binding of E2020 (Aricept (R)) to cholinesterases. *Eur. J. Biochem.* **2003**, *270*, 4447-4458.
- (34) Lee, E. C.; Kim, D.; Jurecka, P.; Tarakeshwar, P.; Hobza, P.; Kim, K. S., Understanding of assembly phenomena by aromatic-aromatic interactions: benzene dimer and the substituted systems. *J. Phys. Chem. A* **2007**, *111*, 3446-3457.
- (35) Rizzo, S.; Bartolini, M.; Ceccarini, L.; Piazzzi, L.; Gobbi, S.; Cavalli, A.; Recanatini, M.; Andrisano, V.; Rampa, A., Targeting Alzheimer's disease: novel indanone hybrids bearing a pharmacophoric fragment of AP2238. *Bioorg. Med. Chem.* **2010**, *18*, 1749-1760.
- (36) Sugimoto, H.; Tsuchiya, Y.; Sugumi, H.; Higurashi, K.; Karibe, N.; Iimura, Y.; Sasaki, A.; Kawakami, Y.; Nakamura, T.; Araki, S.; Yamanishi, Y.; Yamatsu, K., Novel piperidine-derivatives - Synthesis and antiacetylcholinesterase activity of 1-Benzyl-4-[2-(N-benzoylamino)ethyl]piperidine derivatives. *J. Med. Chem.* **1990**, *33*, 1880-1887.
- (37) Kwon, Y. E.; Park, J. Y.; No, K. T.; Shin, J. H.; Lee, S. K.; Eun, J. S.; Yang, J. H.; Shin, T. Y.; Kim, D. K.; Chae, B. S.; Leem, J. Y.; Kim, K. H., Synthesis, in vitro assay, and molecular modeling of new piperidine derivatives having dual inhibitory potency against acetylcholinesterase and A beta(1-42) aggregation for Alzheimer's disease therapeutics. *Bioorg. Med. Chem.* **2007**, *15*, 6596-6607.
- (38) Piazzzi, L.; Cavalli, A.; Belluti, F.; Bisi, A.; Gobbi, S.; Rizzo, S.; Bartolini, M.; Andrisano, V.; Recanatini, M.; Rampa, A., Extensive SAR and computational studies of 3-{4-[(benzylmethylamino)methyl]phenyl}-6,7-dimethoxy-2H-2-chromenone (AP2238) derivatives. *J. Med. Chem.* **2007**, *50*, 4250-4254.

- (39) Cockroft, S. L.; Perkins, J.; Zonta, C.; Adams, H.; Spey, S. E.; Low, C. M. R.; Vinter, J. G.; Lawson, K. R.; Urch, C. J.; Hunter, C. A., Substituent effects on aromatic stacking interactions. *Org. Biomol. Chem.* **2007**, *5*, 1062-1080.
- (40) Arnstein, S. A.; Sherrill, C. D., Substituent effects in parallel-displaced pi-pi interactions. *Phys. Chem. Chem. Phys.* **2008**, *10*, 2646-2655.
- (41) Ringer, A. L.; Sinnokrot, M. O.; Lively, R. P.; Sherrill, C. D., The effect of multiple substituents on sandwich and T-Shaped pi-pi interactions. *Chem.-Eur. J.* **2006**, *12*, 3821-3828.
- (42) Berg, L.; Andersson, C. D.; Artursson, E.; Hörnberg, A.; Tunemalm, A. K.; Linusson, A.; Ekström, F., Targeting acetylcholinesterase: identification of chemical leads by high throughput screening, structure determination and molecular modeling. *PLoS One* **2011**, *6*, e26039.
- (43) Ellman, G. L.; Courtney, K. D.; Andres, V.; Featherstone, R. M., A new and rapid colorimetric determination of acetylcholinesterase activity. *Biochem. Pharmacol.* **1961**, *7*, 88-95.
- (44) Araújo, J. Q.; de Brito, M. A.; Hoelz, L. V. B.; de Alencastro, R. B.; Castro, H. C.; Rodrigues, C. R.; Albuquerque, M. G., Receptor-dependent (RD) 3D-QSAR approach of a series of benzylpiperidine inhibitors of human acetylcholinesterase (HuAChE). *Eur. J. Med. Chem.* **2011**, *46*, 39-51.
- (45) Biela, A.; Nasief, N. N.; Betz, M.; Heine, A.; Hangauer, D.; Klebe, G., Dissecting the hydrophobic effect on the molecular level: the role of water, enthalpy, and entropy in ligand binding to thermolysin. *Angew. Chem. Int. Ed.* **2013**, *52*, 1822-1828.
- (46) Reynolds, C. H.; Holloway, M. K., Thermodynamics of ligand binding and efficiency. *Acs Med. Chem. Lett.* **2011**, *2*, 433-437.
- (47) Berg, L.; Niemiec, M. S.; Qian, W. X.; Andersson, C. D.; Wittung-Stafshede, P.; Ekström, F.; Linusson, A., Similar but different: thermodynamic and structural characterization of a pair of enantiomers binding to acetylcholinesterase. *Angew. Chem. Int. Ed.* **2012**, *51*, 12716-12720.
- (48) Calculated on inhibitor structures from chain A in the crystal structures.

- (49) Seo, J. I.; Kim, I.; Lee, Y. S., pi-pi Interaction energies in monosubstituted-benzene dimers in parallel- and antiparallel-displaced conformations. *Chem. Phys. Lett.* **2009**, *474*, 101-106.
- (50) Wallnoefer, H. G.; Fox, T.; Liedl, K. R.; Tautermann, C. S., Dispersion dominated halogen-pi interactions: energies and locations of minima. *Phys. Chem. Chem. Phys.* **2010**, *12*, 14941-14949.
- (51) Matter, H.; Nazare, M.; Gussregen, S.; Will, D. W.; Schreuder, H.; Bauer, A.; Urmann, M.; Ritter, K.; Wagner, M.; Wehner, V., Evidence for C-Cl/C-Br center dot center dot center dot pi Interactions as an important contribution to protein-ligand binding affinity. *Angew. Chem. Int. Ed.* **2009**, *48*, 2911-2916.
- (52) Ekström, F.; Pang, Y. P.; Boman, M.; Artursson, E.; Akfur, C.; Börjegen, S., Crystal structures of acetylcholinesterase in complex with HI-6, Ortho-7 and obidoxime: structural basis for differences in the ability to reactivate tabun conjugates. *Biochem. Pharmacol.* **2006**, *72*, 597-607.
- (53) This also served to confirm the long-term stability of our protein batches.
- (54) *Origin SR4 7.0552*; Origin lab corporation: One roundhouse plaza, Northampton, MA 01060, USA.
- (55) Ekström, F.; Akfur, C.; Tunemalm, A. K.; Lundberg, S., Structural changes of phenylalanine 338 and histidine 447 revealed by the crystal structures of tabun-inhibited murine acetylcholinesterase. *Biochemistry* **2006**, *45*, 74-81.
- (56) Kabsch, W., Automatic processing of rotation diffraction data from crystals of initially unknown symmetry and cell constants. *J. Appl. Crystallogr.* **1993**, *26*, 795-800.
- (57) Murshudov, G. N.; Vagin, A. A.; Dodson, E. J., Refinement of macromolecular structures by the maximum-likelihood method. *Acta Crystallogr., Sect. D: Biol. Crystallogr.* **1997**, *53*, 240-255.
- (58) Adams, P. D.; Grosse-Kunstleve, R. W.; Hung, L. W.; Ioerger, T. R.; McCoy, A. J.; Moriarty, N. W.; Read, R. J.; Sacchettini, J. C.; Sauter, N. K.; Terwilliger, T. C., PHENIX: building new

software for automated crystallographic structure determination. *Acta Crystallogr., Sect. D: Biol. Crystallogr.* **2002**, 58, 1948-1954.

- (59) Emsley, P.; Cowtan, K., Coot: model-building tools for molecular graphics. *Acta Crystallogr., Sect. D: Biol. Crystallogr.* **2004**, 60, 2126-2132.
- (60) Vriend, G., WHAT IF: a molecular modelling and drug design program. *J. Mol. Graphics* **1990**, 8, 52-56.
- (61) DeLano, W. L., The PyMOL Molecular Graphics System. **2002**.

Table of Contents graphic

